





Cite this: *Dalton Trans.*, 2023, **52**, 10423

# Enhanced adsorption–catalysis combination for the removal of sulphur from fuels using polyoxometalates supported on amphiphatic hybrid mesoporous silica nanoparticles†

Josefa Ortiz-Bustos, <sup>a</sup> Helena Pérez del Pulgar, <sup>a</sup> Yolanda Pérez <sup>\*a,b</sup> and Isabel del Hierro <sup>\*a</sup>

Polyoxometalate (POM) mesoporous silica-based materials with a low POM loading have been designed with hydrophilic and hydrophobic properties. These materials act as powerful heterogeneous catalysts in oxidative desulfurization (ODS), owing to their ability to adsorb both H<sub>2</sub>O<sub>2</sub> and sulphur-containing compounds from the model oil simultaneously. The formation of charge transfer salts through ion pair interaction with a choline functionality, available on the hybrid silica support, affords robust and recyclable heterogeneous catalysts for the ODS process under mild conditions (45 min and 40 °C). Besides, the nature of the polyoxometalate anions is highly dependent on the characteristics of the silica surface. The masking of silanol groups present on the silica surface using silylating agents, with diverse reactivity and steric hindrance, influences the silica surface–heteropolyanion interactions, as well as heteropolyanion–heteropolyanion interactions. In addition, it modifies the hydrophobic properties of the surface, which is a determining factor in the adsorption properties of non-polar dibenzothiophene (DBT) by the catalysts. Adsorption, an anterior step to the oxidation reaction, has been demonstrated to be key to the superior activity of POM–SiMe<sub>3</sub>–Chol–MSN, where the silanol groups have been capped by trimethylsilyl groups. For the first time, and to better understand POM–surface and POM–POM anion interactions, an extensive characterization of the materials has been performed using <sup>13</sup>C, <sup>31</sup>P, and <sup>95</sup>Mo MAS NMR spectroscopy and solid-state electrochemical techniques, among others.

Received 5th June 2023,  
Accepted 30th June 2023  
DOI: 10.1039/d3dt01725g

rsc.li/dalton

## 1. Introduction

Polyoxometalates (POM) have interesting redox properties, so they have been used as catalysts, photocatalysts and electrocatalysts<sup>1–5</sup> and, as promising active materials in the production of biomass and energy storage.<sup>6</sup> Their behaviour as Brønsted/Lewis acids due to the presence of high oxidation state metal centres and donor oxygen atoms and their great stability against degradation make them suitable candidates to be used in several catalytic applications. Immobilization of this class of inorganic compounds has become the most common method for their dispersal on solid supports and

hence takes advantage of their properties in heterogeneous catalysis. The immobilization of polyoxometalates avoids one of the most important drawbacks of this inorganic catalyst in the homogeneous phase, namely its recovery and reuse. For instance, in oxidative desulfurization in a liquid phase, a transfer agent is commonly required to exchange the peroxy-polyoxometalate species from the aqueous phase containing the oxidant (H<sub>2</sub>O<sub>2</sub>) to the substrate containing the organic or oil phase. Separating these homogeneous catalysts from the oil phase after desulfurization and aggregate formation with the phase transfer agent can be difficult due to their high solubility in the fuel phase. In contrast, in the heterogeneous phase, the catalyst can be recovered and reused, preventing fuel impurification.

The use of hybrid organic–inorganic mesoporous silica has been exploited by several authors to prepare highly stable and solvent-tolerant heterogeneous catalysts.<sup>7</sup> One widely implemented strategy has been the synthesis of zwitterionic supports for the efficient immobilization of Keggin-type heteropolyacids (HPAs), mainly phosphotungstic and phosphomolybdic acids. HPAs strongly interact with protonated

<sup>a</sup>Departamento de Biología y Geología, Física y Química Inorgánica, Escuela Superior de Ciencias Experimentales y Tecnología, Universidad Rey Juan Carlos, 28933 Móstoles, Madrid, Spain. E-mail: isabel.hierro@urjc.es, yolanda.cortes@urjc.es

<sup>b</sup>Advanced Porous Materials Unit, IMDEA Energy, Av. Ramón de la Sagra 3, 28935 Móstoles, Madrid, Spain

† Electronic supplementary information (ESI) available. See DOI: <https://doi.org/10.1039/d3dt01725g>



organic species derived from N aliphatic and aromatic amines and with quaternary ammonium groups forming ion pairs and producing robust highly recyclable heterogeneous catalysts. An early example is the material  $\equiv\text{Si}(\text{CH}_2)_3\text{NH}_3\text{-HPA}$  synthesized by Kaleta and co-workers, in which an aminopropyl functionalized MCM-41 material was used to achieve efficient anchoring of heteropolyanions and prevent HPA leaching when applied as a catalyst in polar solvent media.<sup>8</sup> Following this path, several authors have taken advantage of the immobilization of silane-based ionic liquids such as propyl-3-ethoxysilyl-3-methylimidazolium chloride ionic liquid<sup>9</sup> or *N*-trimethoxysilylpropyl-*N,N,N*-trimethylammonium chloride<sup>10</sup> to prepare the appropriate hybrid organic–inorganic mesoporous silica prior to HPA immobilization.

In previous work, our group performed the immobilization of phosphomolybdic acid on different supports (hybrid mesoporous silica and  $\text{TiO}_2$ ) using surface organometallic chemistry strategies with the aim to understand the role of Si–OH, Si–OR or Ti–OH groups. Our results showed that the electronic properties of POM can be tuned according to the nature of the support.<sup>11</sup> Here we further proceeded with these studies, and used mesoporous silica nanospheres modified with a choline hydroxide-based ionic liquid as a support to guarantee the formation of a strong ion pair interaction with the polyoxometalate anion. In addition, and simultaneously, we used a capping agent to mask the unreacted silanol groups (trimethoxymethylsilane, hexamethyldisilazane, phenyltriethoxysilane or 2-(diphenylphosphino)ethyltriethoxysilane) and to modify the hydrophobic–hydrophilic properties of the surface. The aim was to investigate how both the silica surface–heteropolyanion and heteropolyanion–heteropolyanion interactions may influence the ODS process. The sulfur removal efficiency and recyclability of these materials have been tested without co-solvent and using  $\text{H}_2\text{O}_2$  as a green oxidant under mild conditions (40 °C). Desulfurization test results show that the as-prepared POM-based heterogeneous catalysts with a low POM loading (7.5 wt% of theoretical phosphomolybdic acid) (POM-R-Chol-MSN where R = Me,  $\text{SiMe}_3$ , Ph, and  $\text{CH}_2\text{CH}_2\text{PPh}_2$ ) show high activity due to the presence of POM moieties and good reusability due to molybdenum species stability upon immobilization.

## 2. Experimental

### 2.1. Preparation of hybrid mesoporous silica nanoparticles functionalized with a choline hydroxide ionic liquid and a capping agent using a post-synthesis procedure (R-Chol-MSN)

Mesoporous silica nanoparticles (MSN) were synthesized according to previously published procedures.<sup>12</sup> Then, 1.0 g of MSN was dehydrated for 16 h at 200 °C and suspended in 30 mL of dried toluene with 2 mmol of 3-(glycidyoxypropyl)trimethoxysilane and stirred vigorously at 85 °C for 30 minutes. 1 mmol of the capping agent (trimethoxymethylsilane, hexamethyldisilazane, phenyltriethoxysilane or 2-(diphenylphosphino)ethyltriethoxysilane) was then added and the suspen-

sion was stirred for 24 h. Subsequently, the solid was filtered, washed with dichloromethane, and dried under vacuum. Polyoxometalates anchored on amphipathic hybrid mesoporous silicas have been synthesized. The heterogeneous catalyst is able to adsorb DBT and  $\text{H}_2\text{O}_2$  in the interface of oil and aqueous phases and can be easily recovered and reused. The mixture was stirred at 50 °C for 48 h. Finally, the white solid, R-Chol-MSN, was isolated by filtration, washed with ethanol, and dried under vacuum.

### 2.2. Functionalization of R-Chol-MSN with phosphomolybdic acid (POM-R-Chol-MSN)

1.0 g of R-Chol-MSN was suspended in 30 mL of ethanol and  $\text{H}_3[\text{PMo}_{12}\text{O}_{40}]$  (0.2 mmol, 20% ethanol) was added. The yellow mixture was dispersed in ethanol and stirred for 2 h in a cold bath. The solid was isolated by filtration and washed with ethanol. For its storage, the catalyst was dried under vacuum. The samples obtained using trimethoxymethylsilane, hexamethyldisilazane, phenyltriethoxysilane or 2-(diphenylphosphino)ethyltriethoxysilane as a capping agent were named POM-R-Chol-MSN (R = Me,  $\text{SiMe}_3$ , Ph, and  $\text{CH}_2\text{CH}_2\text{PPh}_2$ ), respectively. For comparison purposes, a sample with unprotected silanol surface groups was also prepared and named POM-Chol-MSN.

### 2.3. Oxidative desulfurization

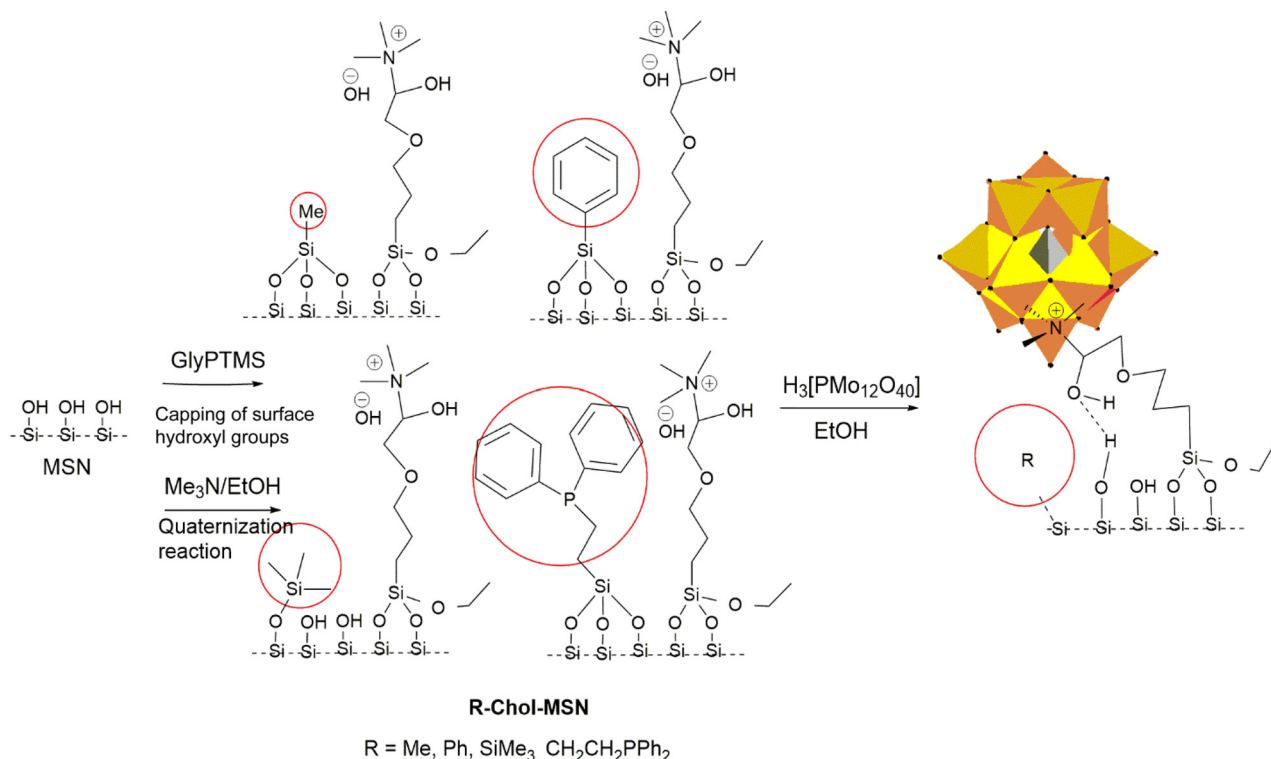
In a typical experiment, the polyoxometalate-based heterogeneous catalyst (1 mol%) was added to 10 mL of the model oil containing dibenzothiophene (DBT) and *n*-octane (S-concentration of 250 ppm) using a Multimax™ Mettler Toledo reactor. Then, 24  $\mu\text{L}$  of a 30%  $\text{H}_2\text{O}_2$  solution (O/S ratio 6) was added to the suspension under stirring and the mixture was heated at 40 °C. In set periods, the stirring was stopped, and 0.5 mL of the liquid was collected and analyzed by gas chromatography with a flame ionization detector (FID) with dodecane being used as an external standard for the quantification of DBT. The sulfone product was also identified by liquid  $^1\text{H}$  NMR spectroscopy. For the recycling experiments, the catalyst POM- $\text{SiMe}_3$ -Chol-MSN was separated by centrifugation, washed, and used in repeated experiments without further treatment.

## 3. Results and discussion

### 3.1. Synthesis

Hybrid inorganic–organic mesoporous silica nanospheres with the choline hydroxide functionality have been synthesized previously by our group<sup>13</sup> and used as a zwitterionic support for the efficient immobilization of polyoxometalates. The choline hydroxide group allows the straightforward acid–base reaction with phosphomolybdic acid in organic media to yield immobilized POMs, moreover, electrostatic interactions are established with the ammonium groups covalently grafted on the silica surface. This strategy aims to produce well-distributed and well-defined surface species, where the protons remaining





**Scheme 1** The immobilization procedure of the polyoxometalate (POM) on hybrid organic–inorganic mesoporous materials. (GlyPTMS = glycidoxypropyltriethoxysilane and surface hydroxyl group capping agent = trimethoxymethylsilane, phenyltriethoxysilane, hexamethyldisilazane and 2-(diphenylphosphino)ethyltriethoxysilane.)

in the molybdenum cluster can be displaced around the structure and may establish hydrogen bonds with the hydroxyl group available in the choline tethered ligand or with the surface silanol groups (see Scheme 1). The additional use of a capping agent capable of masking totally or partially the unreacted silanol groups on the silica surface is attempted to investigate the existence of additional interactions such as surface–anion or anion–anion interactions. Also, the incorporation of a capping agent is helpful to tune the hydrophobicity of the material surface and the steric hindrance imposed by the alkyl or aryl substituents on the formation of the above-mentioned anion–surface interactions.

### 3.2. Characterization of catalysts

Nitrogen adsorption–desorption isotherms of the polyoxometalate-based materials were recorded, and the findings are illustrated in Fig. S1.† Pristine MSN show a type IV isotherm according to IUPAC, which is consistent with a mesoporous material with parallel cylindrical pores in a 2D hexagonal structure. The hybrid mesoporous silica materials POM-R-Chol-MSN show a type III isotherm with an H1 hysteresis loop centered at  $P/P_0 > 0.9$ . Textural properties such as the surface area ( $S_{\text{BET}}$ ), total pore volume ( $V_p$ ) and BJH pore diameter ( $D_p$ ) were obtained from  $N_2$  isotherms (Table 1). All POM-R-Chol-MSN materials show an important reduction in the textural property values in comparison with naked MSN or hybrid

Chol-MSN. The high loading of choline moieties and sterically demanding phosphomolybdate anions suggest their incorporation into the entrance of the channel and hence the blocking of the nitrogen molecules. Since the pore volume and pore size are very similar for all the functionalized materials, the catalytic process studied probably takes place mainly in the outermost silica surface.

The phosphomolybdate anion contents were calculated based on X-ray fluorescence analysis (XRF) and are included in Table 1. To corroborate the heteropolyanion contents ICP measurements were also performed for some representative samples obtaining slightly lower heteropolyanion contents (see Table S1†). With the heteropolyanion loading being calculated from XRF analysis ( $L_o = \% \text{ Mo} / (12 \times \text{molybdenum atomic weight})$ ) and  $S_{\text{BET}}$  of the samples, the average surface density of the attached POM molecules and the average intermolecular distance were also calculated. As expected, the modified MSN samples have a low molecule surface density in the range of 0.07–0.13 molecule per  $\text{nm}^2$  and a high intermolecular distance from 2.83 to 3.72 nm. These values are consistent with the formation of charge transfer complexes like  $(\text{Chol})_2[\text{HPMo}_{12}\text{O}_{40}]$  and/or  $(\text{Chol})_3[\text{PMo}_{12}\text{O}_{40}]$ . However, the presence of unreacted choline hydroxide units on the silica surface cannot be ignored.<sup>11</sup>

The thermal behavior of POM-SiMe<sub>3</sub>-Chol-MSN and related materials such as POM-Chol-MSN and Chol-HMDS-MSN was



**Table 1** Textural properties, heteropolyanion loading, surface density, intermolecular distance, Mo<sup>6+</sup>/Mo<sup>5+</sup> ratio, and  $\zeta$  potential values of the synthesized materials

Material	$S_{\text{BET}}$ (m <sup>2</sup> g <sup>-1</sup> )	Pore volume (cm <sup>3</sup> g <sup>-1</sup> )	Heteropolyanion loading ( $L_0$ ) <sup>a</sup> (mmol g <sup>-1</sup> )	Average intermolecular distance (nm)	Average surface density (molec. per nm <sup>2</sup> )	Mo <sup>6+</sup> /Mo <sup>5+</sup> ratio (XPS)	$\zeta$ potential <sup>b</sup> (eV)
MSN	1042	1.32	—	—	—	—	From -20 to -30 <sup>14,15</sup>
Chol-MSN	825	0.50	—	—	—	—	-4.8
POM-Chol-MSN	32.0	0.17	0.14	3.46	0.08	1.67	-6.2
POM-Me-Chol-MSN	24.6	0.16	0.20	2.94	0.12	1.49	-10.7
POM-Ph-Chol-MSN	23.3	0.18	0.16	3.34	0.09	1.36	-15.0
POM-SiMe <sub>3</sub> -Chol-MSN	24.2	0.19	0.13	3.72	0.07	1.20	-7.7
POM-CH <sub>2</sub> CH <sub>2</sub> PPh <sub>2</sub> -Chol-MSN	19.6	0.16	0.22	2.83	0.13	1.65	-13.2

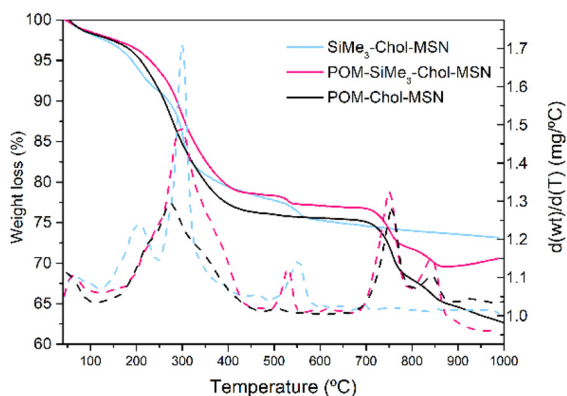
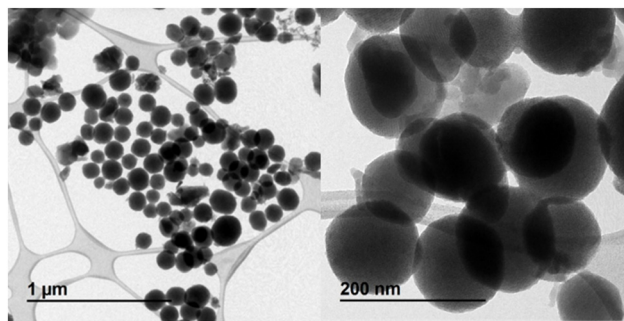
<sup>a</sup>The heteropolyanion loading was obtained by X-ray fluorescence analysis (XRF) ( $L_0 = \% \text{ Mo} \times 10 / (12 \times \text{molybdenum atomic weight})$ ). <sup>b</sup>1 mg mL<sup>-1</sup>, pH = 7 water Milli-Q (average three independent measurements).

studied by thermogravimetric and differential thermal analysis (TGA and DTA) (Fig. 1). TGA curves exhibit a small weight loss at around 100 °C due to the physisorbed water on the surface's samples. Then, a weight loss region is found from 160 to 400 °C corresponding to the decomposition of organic moieties anchored to surface silica, and a sharp peak is observed at 500 °C associated with the additional decomposition of trimethylsilyl groups anchored to the silica surface, Me<sub>3</sub>Si-O-Si≡. Finally, two exothermic peaks at 755 and 845 °C were observed in the DTA curves ascribed to POM decomposition to render MoO<sub>3</sub>.

Small-angle XRD studies show that the pristine MSN material has a typical well-resolved pattern at low  $2\theta$  values with three characteristic peaks: one strong (100) at 2.4 and two lower (110) and (200) at 4.1 and 4.8, respectively; corresponding to a highly ordered mesoporous silica (Fig. S2†). The hybrid material, Chol-MSN, suffers an important reduction in the main peak intensity at 2.44 and the peaks (110) and (200) disappear. This also occurred in the POM-Chol-MSN sample. The intensity decrease of the diffraction plane (100) is explained by changes in the wall thickness due to the ongoing functionalization process on the surface of the nanoparticles and the probable blocking of pores as N<sub>2</sub> adsorption analysis

suggests. SEM and TEM micrographs show that the spherical framework of MSN is well preserved after functionalization and POM-Chol-MSN mesoporous silica spheres are uniform in shape and diameter size (Fig. 2).

**3.2.1. Characterization by FTIR and DR-UV-Vis spectroscopy.** FTIR spectra of all samples were recorded, and the results are shown in Fig. 3 and Fig. S3.† The characteristic bands of the physisorbed water molecules appear at 3432 cm<sup>-1</sup> and 1637 cm<sup>-1</sup> corresponding to O-H stretching and deformation vibrations, respectively. Silica-based materials show other typical sharp bands attributed to the Si-O stretching vibrations at 1086, 962, and 808 cm<sup>-1</sup>. The incorporation of choline-based functionality used to anchor the POM anions adds new bands to the spectra corresponding to  $\nu(\text{C-H})$  stretching vibrations at 2937 and 2881 cm<sup>-1</sup> and two nearby bands at 1487 and 1476 cm<sup>-1</sup> attributed to the bending vibrations of  $\delta(\text{C-H})$  of the tetraalkylammonium group of the choline unit. In addition, in the silylated materials new bands are observed due to the incorporation of capping ligands, as an example, the trimethylsilyl group shows a signal at 845 cm<sup>-1</sup> assigned to the Si-CH<sub>3</sub> antisymmetric deformation stretch. Both the silylated and unsilylated silicas display a silanol band in the region of 3700–3200 cm<sup>-1</sup>. However, the silylated material showed a very significant decrease in the silanol band. This result is mainly due to the conversion of

**Fig. 1** TGA and DTA analysis curves for POM-Chol-MSN, POM-SiMe<sub>3</sub>-Chol-MSN, and SiMe<sub>3</sub>-Chol-MSN materials.**Fig. 2** SEM and TEM micrographs of POM-Chol-MSN as a representative sample.



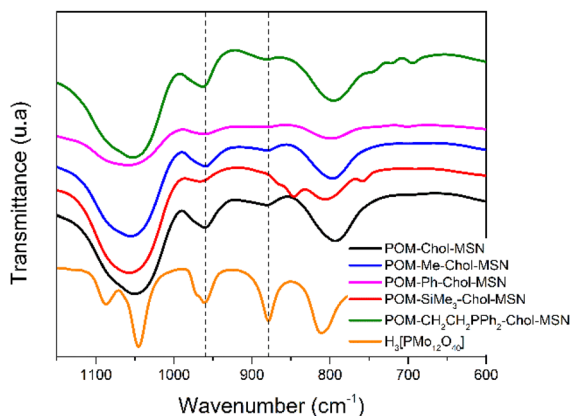


Fig. 3 FTIR spectra of POM-based materials in comparison with that of  $\text{H}_3[\text{PMo}_{12}\text{O}_{40}]$ .

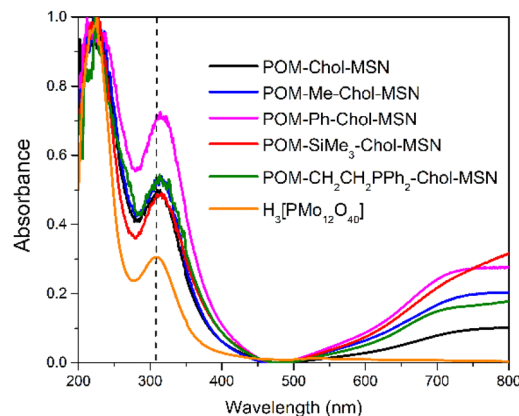


Fig. 4 DRUV-vis spectra of POM-based materials in comparison with that of  $\text{H}_3[\text{PMo}_{12}\text{O}_{40}]$ .

silanols into trimethylsilyl groups, but it is also likely to be due to diminished water adsorption because of an increase in hydrophobicity (Fig. S3<sup>†</sup>). In FTIR spectra of POM mesoporous silica-based materials, some of the most representative bands from the polyoxometalate units appear overlapped due to the intense stretching vibration of the hybrid silica support, but even so interesting differences could be inferred. Fig. 3, displays the spectra of the materials focused on the region where  $\text{Mo}=\text{O}_t$  ( $\text{O}_t$  is terminal oxygen) and  $\text{Mo}-\text{O}_b-\text{Mo}$  ( $\text{O}_b$  is bridging oxygen) signals appear at around 963 and 882  $\text{cm}^{-1}$ , respectively. All the materials show a similar pattern of signals, which indicates the maintenance of the symmetry of the Keggin-type structure upon immobilization. The signal due to  $\text{Mo}-\text{O}_b-\text{Mo}$  is observed for all materials except for POM-SiMe<sub>3</sub>-Chol-MSN. The signal attributed to  $\text{Mo}=\text{O}_t$  appears at a similar wavenumber to free  $\text{H}_3[\text{PMo}_{12}\text{O}_{40}]$  but it shifts to a higher wavenumber in the case of POM-SiMe<sub>3</sub>-Chol-MSN, which according to some authors, is caused by the increasing of the distance between adjacent heteropolyanions and the weakening of the electrostatic interactions between heteropolyanions.<sup>16</sup> For this type of material, POM immobilization depends on other factors besides the electrostatic interactions established with the choline-based functionality. The anchored heteropolyanions may interact with the silica surface and may establish anion-anion interactions. Our previous results based on FTIR studies disclosed that the POM moiety signals were broader and less intense in unmasked materials, suggesting stronger interactions between POM anions and Si-OH surface groups in comparison with Si-R groups.<sup>11</sup> This new set of materials supports these results, and it also shows a stronger effect of silanization with the hexamethyldisilazane reactant in POM-SiMe<sub>3</sub>-Chol-MSN in comparison with other used masking organosilanes.

To gain further knowledge about the electronic structure, DRUV-Vis measurements were performed. As can be seen in Fig. 4, two strong signals appear in all samples at 220–240 nm and 305–317 nm. The reflectance band between 220–240 nm is attributed to the ligand-metal charge transfer (LMCT) transition from terminal oxygen to molybdenum atoms ( $\text{Mo}=\text{O}_t$ ).

The band located at 305–317 nm corresponds to the presence of  $\text{Mo}-\text{O}_b-\text{Mo}$  and the LMCT type transition between bridging oxygen atoms and molybdenum.<sup>17</sup> The synthesized POM-R-Chol-MSN materials, which were stored under sunlight, suffered a colour change from yellow to blue a few hours after being prepared. This indicates the presence of Mo(v) in the Keggin anion, and suggests that exposure to sunlight induces the reduction of  $[\text{PMo}_{12}\text{O}_{40}]^{m-}$  to  $[\text{XPMo}_{11}\text{Mo}^{\text{V}}\text{O}_{40}]^{(m+1)-}$ . In all the reflectance spectra the appearance of an additional band at around 750 nm supports the proposal of the partial reduction of immobilized POM heteropolyanions under sunlight storage.

Photochromic properties of these charge-transfer salts are closely related to the reduction potential of the polyoxoanions, acting as electron-accepting anions, and to the donor properties of the electron-rich organic cations. In this family of materials, choline-based moieties anchored to the hybrid silica-based materials must play a similar role by rendering  $(\text{Chol})_2[\text{HPMo}_{12}\text{O}_{40}]$  and/or  $(\text{Chol})_3[\text{PMo}_{12}\text{O}_{40}]$  tethered complexes.<sup>18</sup> In the spectra, the reflectance bands attributed to ( $\text{Mo}=\text{O}_t$ ) and ( $\text{Mo}-\text{O}_b-\text{Mo}$ ) appear red-shifted in comparison with free  $\text{H}_3[\text{PMo}_{12}\text{O}_{40}]$  (Fig. S5<sup>†</sup>), which indicates that both terminal and bridging oxygen-molybdenum bonds are equally affected after immobilization.

Taking into account molybdenum loading values and the relative molecular distance calculated and presented in Table 1, it could be accepted that the red shift observed for  $\text{O}^{2-} \rightarrow \text{Mo}^{6+}$  is proportional to the number of supported polyoxometalates in POM-R-Chol-MSN materials, and hence it would be related to the nature of the support and the relative distance between anions. However, POM-SiMe<sub>3</sub>-Chol-MSN with a similar molybdenum loading and an intermolecular distance to POM-Chol-MSN, seems to behave differently, the only change being the hydrophobic -SiMe<sub>3</sub> groups present on the silica surface. These results suggest the influence of several factors on the position of DRUV-Vis bands of the POM anion after immobilization, such as the counterion, anion-anion interactions, and surface-anion interactions.



**3.2.2. Characterization by nuclear magnetic resonance and XPS.** The  $^{13}\text{C}$  MAS NMR spectra recorded support the immobilization of both the ligand with the choline functionality and the organosilane used for the controlled silanization of free silanol surface groups. As can be seen in Fig. 5, the spectrum of POM-Chol-MSN shows signals at 8, 24, and 72 ppm, due to the carbon atoms of the propyl chain  $-\text{Si}-\text{CH}_2-$ ,  $-\text{CH}_2-\text{CH}_2-\text{CH}_2-$  and  $-\text{CH}_2-\text{CH}_2-\text{CH}_2-\text{O}-$ , respectively. The signal attributed to the methylene group  $-\text{O}-\text{CH}_2-\text{CHOH}-$  appears at 72 ppm (overlapped), and the signals due to carbon atoms of the opened epoxide function appear at 66 and 72 ppm, for the methyne  $-\text{CH}-\text{OH}$  and methylene  $-\text{N}-\text{CH}_2-$  groups, respectively. Two additional peaks were observed at 15 and 59 ppm and assigned to the unreacted ethoxide group of the organic ligand  $\text{CH}_3\text{CH}_2-\text{O}-$ , since the methoxide groups on the starting 3-(glycidyloxypropyl)trimethoxysilane reactant have been replaced by ethoxide because the quaternization reaction is performed in ethanol. Finally, the intense resonance peak at *ca.* 54 ppm indicates the presence of methyl groups of the quaternary ammonium group  $(\text{CH}_3)_3\text{N}^+\text{CH}_2-$ .

The rest of the materials show a similar pattern of signals for the choline-based ligand and additional representative signals of the silylating agents used to mask the unreacted  $\text{Si}-\text{O}-\text{H}$  groups on the surface. The surface groups are converted into the trimethylsilyl group  $(\text{Me}_3\text{Si}-\text{O}-\text{Si}\equiv)$  by the reaction with  $(\text{HN}(\text{SiMe}_3)_2)$ , methyl groups  $(\text{Me}-\text{Si}\equiv)$  by the reaction with  $(\text{MeSi}(\text{OMe})_3)$ , phenyl  $(\text{Ph}-\text{Si}\equiv)$  groups by the reaction with  $(\text{PhSi}(\text{OEt})_3)$ , and (diphenylphosphine)ethyl groups  $(\text{PPh}_2-\text{CH}_2-\text{CH}_2-\text{Si}\equiv)$  by the reaction with  $(\text{PPh}_2\text{CH}_2\text{CH}_2\text{Si}(\text{OEt})_3)$ , respectively. As can be observed in Fig. 5, the most distinctive signals appear at  $\delta = -2.6$  ppm due to the trimethylsilyl group in POM-SiMe<sub>3</sub>-Chol-MSN, and at  $\delta = -5.9$  ppm due to the methyl group in POM-Me-Chol-MSN. Finally, at the lower field, the signals attributed to the phenyl group in POM-Ph-Chol-MSN appear in the range  $\delta = 127-132$  ppm, and the signals due to the phenyl groups attached to the phos-

phorus atom, appear at around  $\delta = 130$  ppm in POM- $\text{CH}_2\text{CH}_2\text{PPh}_2$ -Chol-MSN.

$^{31}\text{P}$  MAS-NMR is a very sensitive technique for identifying the local phosphorus chemical environment and surrounding symmetry, which can be used to obtain extra information about the changes in the chemical environment of POM moieties after their immobilization. In our previous studies, we concluded that the  $^{31}\text{P}$  MAS-NMR for POM-Chol-MSN was consistent with the presence of Keggin-type anions  $(\text{Chol})_3[\text{PMo}_{12}\text{O}_{40}]$  at  $\delta = -4.8$  ppm and the lacunar anion  $[\text{PMo}_{11}\text{O}_{39}]^{7-}$  at  $\delta = -0.26$  ppm, due to the decomposition (although in small extension) of the phosphomolybdate anion. Keggin-type anions  $(\text{Chol})_3[\text{PMo}_{12}\text{O}_{40}]$  may further interact with the silica surface to give  $(\equiv\text{Si}-\text{OH}_2)_n^+ [[\text{Chol}]_{3-n}\text{Mo}_{12}\text{PO}_{40}]^{n-3}$  at  $\delta = -6.9$  ppm.<sup>19,20</sup>

In this study, the  $^{31}\text{P}$  MAS-NMR spectra recorded for POMs-SiMe<sub>3</sub>-Chol-MSN and POM- $\text{CH}_2\text{CH}_2\text{PPh}_2$ -Chol-MSN samples show an intense signal with a similar chemical shift of  $-3.3$  ppm, that can be attributed to  $(\text{Chol})_3[\text{PMo}_{12}\text{O}_{40}]$  heteropolyanions immobilized by electrostatic interactions (Fig. 6). The latter material also shows two additional weak signals at 1.0 and 1.9 ppm, besides two broad and intense signals in the range of 20–40 ppm, which are attributed to the phenyl phosphine groups. POM-Ph-Chol-MSN and POM-Me-Chol-MSN show a similar spectrum with one intense signal at  $\delta = -3.2$  ppm attributed to  $(\text{Chol})_3[\text{PMo}_{12}\text{O}_{40}]$ , and three additional weak signals being shifted to a higher field at  $\delta = -5.9$ , 0.7 and 1.9 ppm. This pattern of signals is probably due to the interaction of immobilized heteropolyanions with a minimum amount of available silanol groups on the silica surface, forming as previously mentioned  $(\equiv\text{Si}-\text{OH}_2)_n^+ [[\text{Chol}]_{3-n}\text{Mo}_{12}\text{PO}_{40}]^{n-3}$  and the lacunar anion  $[\text{PMo}_{11}\text{O}_{39}]^{7-}$ .

The  $^{31}\text{P}$  MAS-NMR spectra recorded for this family of materials are indicative of the degree of surface coverage accomplished with the different organosilanes used in this

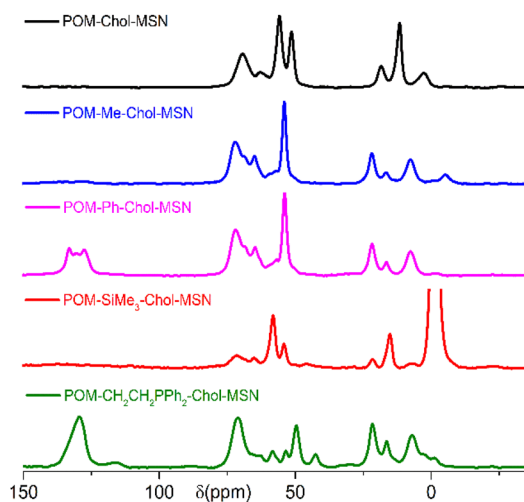


Fig. 5  $^{13}\text{C}$  CP MAS NMR of unsilylated POM-Chol-MSN and silylated POM-R-Chol-MSN materials.

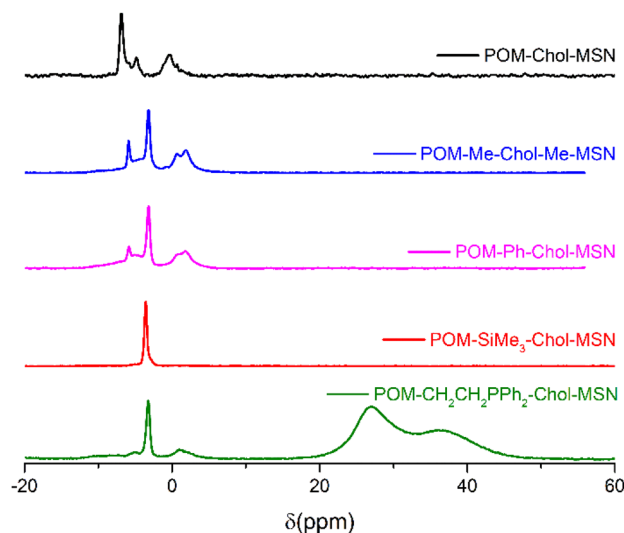


Fig. 6  $^{31}\text{P}$  MAS-NMR of unsilylated POM-Chol-MSN and silylated POM-R-Chol-MSN materials.



study. The most successful method is surface silanization, where the lowest interactions are observed between the polyoxometalate anions and the surface of the support, resulting in higher stability of the  $(\text{Chol})_3[\text{PMo}_{12}\text{O}_{40}]$  moiety formed by ionic pair interactions. In this study, the reaction between Si-OH and  $(\text{Me}_3\text{Si})_2\text{NH}$ , with the formation of ammonia as the only by-product, is a very successful reaction under mild conditions providing efficient coverage. The use of alkoxysilanes such as  $\text{MeSi}(\text{OMe})_3$  and  $\text{PhSi}(\text{OEt})_3$  render a similar degree of coverage although they possess different steric requirements. Although a similar degree of silanization could be expected for  $\text{PPh}_2\text{CH}_2\text{CH}_2\text{Si}(\text{OEt})_3$ , the  $^{31}\text{P}$  MAS-NMR spectrum suggests higher stability for the heteropolyanion in POM- $\text{CH}_2\text{CH}_2\text{PPh}_2$ -Chol-MSN probably due to a weaker interaction with the silica surface. The highest steric hindrance imposed by the bulky diphenyl alkylphosphine groups prevents the interaction of the anion with the support surface.<sup>21,22</sup>

To gain further insights into the molybdenum chemical environment  $^{95}\text{Mo}$  MAS NMR studies were performed. The use of high-field magnets has accelerated the studies of high-resolution solid-state MAS NMR experiments. The new technologies bring higher sensitivity and resolution by increasing equilibrium magnetization and decreasing inhomogeneous broadening due to second-order quadrupole interactions. However,  $^{95}\text{Mo}$  NMR studies are still far away from being considered a routine solid-state characterization technique.<sup>23,24</sup> The study reported by Edwards *et al.*<sup>25</sup> using 94.8% isotopically enriched  $^{95}\text{Mo}$  is noteworthy. In this work, the static powder spectrum for  $\text{H}_3[\text{PMo}_{12}\text{O}_{40}]$  was measured. This spectrum has a broad ( $W_{1/2} = 57.28$  Hz) and a complex signal at 468 ppm which shows the size to which the quadrupolar coupling can grow in an octahedral environment; this large quadrupolar coupling being the result of having six different Mo-O distances in each of the 12 octahedra of the heteropolyanion.

In our experiments,  $^{95}\text{Mo}$  MAS NMR spectra have been performed at a moderate field of 26.05 MHz (9.4 T) at a MAS rate of 12 kHz for  $\text{H}_3[\text{PMo}_{12}\text{O}_{40}]$  and the immobilized POM materials. For  $\text{H}_3[\text{PMo}_{12}\text{O}_{40}]$  the resulting  $^{95}\text{Mo}$  central band resonance is broader than that of  $[\text{Mo}(\text{CO})_6]$  used as a reference compound (Fig. S6<sup>†</sup>), with different singularities in the line shape, and centred at around  $\delta = -239$  ppm.  $\text{H}_3[\text{PMo}_{12}\text{O}_{40}]$  with twelve edges and corner-sharing  $\text{MoO}_6$  octahedra shows a distorted octahedral symmetry and hence enlarged signals, as expected. The  $^{95}\text{Mo}$  MAS NMR spectra measured for the silica-based materials are not straightforward with several signals and patterns extending from 3000 to -2000 ppm. Nevertheless, some conclusions can be inferred. As can be seen in Fig. 7, in all spectra of silylated POM-R-Chol-MSN materials a signal appears at around  $\delta = -506$  ppm that can be attributed to the anchored anion  $[\text{PMo}_{12}\text{O}_{40}]^{3-}$  with  $\text{MoO}_6$  units. This signal shows a significant enlargement (8.4–9.1 kHz) which suggests an important degree of distortion at the molybdenum octahedral site upon immobilization.<sup>26</sup> In the spectrum of the unsilylated POM-Chol-MSN material significant differences are observed. Besides the signal at around  $\delta = -506$  ppm attributed to the  $\text{MoO}_6$  units of the anchored

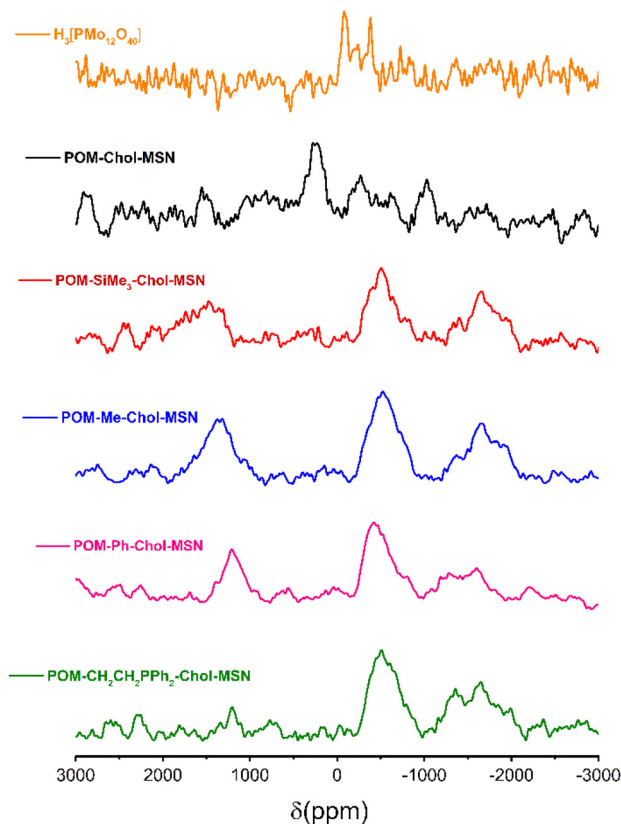


Fig. 7  $^{95}\text{Mo}$  magnetic angle spinning resonance NMR of unsilylated POM-Chol-MSN and silylated POM-R-Chol-MSN materials.

anion  $[\text{PMo}_{12}\text{O}_{40}]^{3-}$ , a more intense signal appears to be shifted to lower fields at 257 ppm, which can be due to  $\text{MoO}_6$  units in  $(\equiv\text{Si}-\text{OH}_2)_n^+ - [(\text{Chol})_{3-n}\text{Mo}_{12}\text{PO}_{40}]^{n-3}$ . It has been reported that the chemical shift variation of  $^{95}\text{Mo}$  can be very wide and it is related to the oxidation state of the metal.<sup>27,28</sup>

In this work, the formation of heteropolyblues is established from UV-Vis and XPS studies. If chemically reduced blue derivatives retained the parent structure with extra delocalized electrons, the signal at around 1350 ppm could be tentatively attributed to  $\text{Mo}^{5+}$  distorted octahedral sites. The reason is that this signal is present in the spectra of those materials with a higher ratio of  $\text{Mo}^{5+}$  sites but is absent in the  $\text{H}_3[\text{PMo}_{12}\text{O}_{40}]$  spectrum, or present with weak intensity in the spectrum of POM- $\text{CH}_2\text{CH}_2\text{PPh}_2$ -MSN which possesses the lowest ratio of  $\text{Mo}^{5+}$ .<sup>29</sup> In addition, the signal that is shielded to higher fields at around -1650 ppm can be tentatively assigned to  $\text{MoO}_{6-x}$  species with lower coordination environments. As previously reported the presence of  $\text{Mo}^{5+}$  sites may justify a change in the coordination environment of molybdenum from six to five coordinated geometry (which could be beneficial for catalytical purposes).<sup>30</sup>

The chemical state and composition of the elements in the materials were analysed by XPS. In Fig. S7,<sup>†</sup> the survey spectra of POM-based materials show that they are composed of C, O, N, P, and Mo elements. The peak deconvolution for Mo 3d is shown in Fig. 8 and Fig. S8.<sup>†</sup> As a representative sample, the



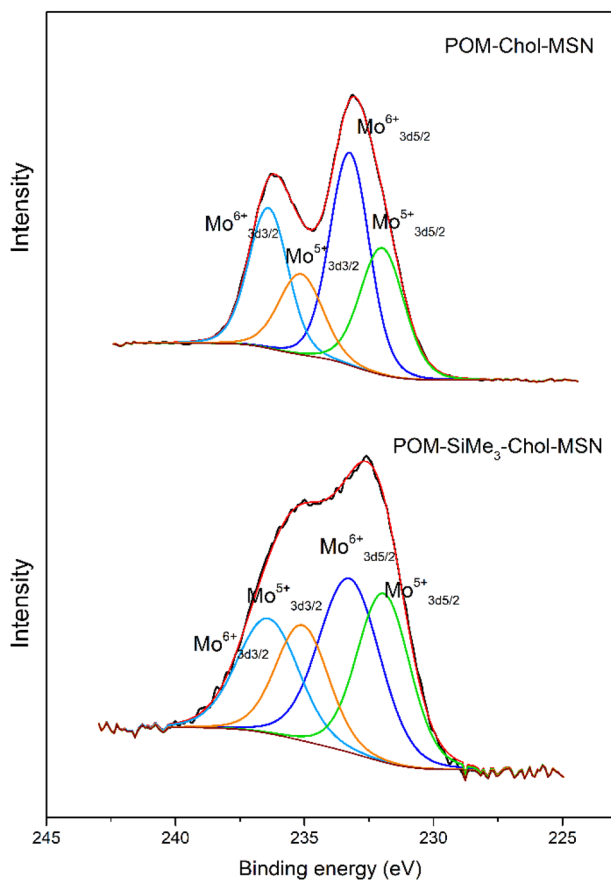


Fig. 8 XPS spectra of Mo 3d for unsilylated POM-Chol-MSN and silylated POM-SiMe<sub>3</sub>-Chol-MSN materials.

XPS spectrum of POM-Chol-MSN displays the peaks located at 233.26 eV and 236.40 eV, which are attributed to Mo 3d<sub>5/2</sub> and Mo 3d<sub>3/2</sub> of Mo<sup>6+</sup>, respectively, while the binding energy doublet at 231.93 eV and 235.08 eV corresponds to Mo<sup>5+</sup> originated by the reduction of part of Mo<sup>6+</sup> to Mo<sup>5+</sup> under sunlight. The XPS analysis supports the co-existence of Mo<sup>6+</sup> and Mo<sup>5+</sup> sites in the prepared materials due to the photochromic properties of the charge transfer salts anchored to the hybrid silica-based materials (Chol)<sub>3</sub>[PMo<sub>12</sub>O<sub>40</sub>]. The Mo<sup>6+</sup>/Mo<sup>5+</sup> ratio in the prepared materials calculated from the corresponding peak area values of deconvoluted XPS spectra ranges from 1.67 to 1.20 eV, the material being POM-SiMe<sub>3</sub>-Chol-MSN which shows the highest ratio of Mo<sup>5+</sup> sites (Table 1).<sup>16</sup>

**3.2.3. Characterization by solid state electrochemical studies.** Since polyoxometalates exhibit rich electrochemistry, we have performed the solid-state electrochemical studies of the (Chol)<sub>3</sub>[PMo<sub>12</sub>O<sub>40</sub>] complex attached to the walls of mesoporous silica materials in acidic media. To do so, modified glassy carbon electrodes were prepared with a mixture of graphite and the material under study and they were used as working electrodes *vs.* an Ag/AgCl/KCl (3 M) reference electrode and a platinum rod as the counter electrode.

The redox chemistry of [PMo<sub>12</sub>O<sub>40</sub>]<sup>3-</sup> is based on the Mo(VI) to Mo(V) reduction accompanied by the uptake of protons to

prevent the build-up of negative charge according to the reaction: [PMo<sub>12</sub>O<sub>40</sub>]<sup>3-</sup> + n e<sup>-</sup> + n H<sup>+</sup> → [H<sub>n</sub>PMo<sub>n</sub><sup>V</sup>Mo<sub>12-n</sub><sup>VI</sup>O<sub>40</sub>]<sup>3-</sup> (n = 2, 4, and 6). As can be seen in Fig. 9, the cyclic voltammogram (CV) of POM-Chol-MSN shows two quasi reversible two-electron consecutive waves at 0.36 and 0.19 V (ΔE = 22 and 20 mV), with a ratio of forward and back current intensity peaks slightly deviating from unity (I<sub>ox</sub>/I<sub>red</sub> = 0.85 and 0.82). This is followed by a third irreversible wave at -0.047 V involving more than two electrons, as can be inferred from the increase in the peak height (ΔE = 36 mV and I<sub>ox</sub>/I<sub>red</sub> = 0.68). The rest of materials POM-R-Chol-MSN (Fig. 9 and Fig. S10<sup>†</sup>) with non-reactive hydrophobic groups on the silica surface shows a similar behaviour with two quasi-reversible redox peaks in the potential range of -0.22 to 0.37 V and a third irreversible peak at around 0 mV. The first two peaks show half-wave potentials E<sub>1/2</sub> very similar to that of unsilylated POM-Chol-MSN with a higher separation between E<sub>cathodic</sub> and E<sub>anodic</sub> (if reversible ΔE should be ≈ 59.1/2) and a lower I<sub>ox</sub>/I<sub>red</sub> ratio, which suggests differences in the kinetics of the processes, with a lower electron transfer rate at the electrode surface.

Linear plots of the current peak *versus* the square root of the scan speed indicate diffusion-controlled processes. However, the correlation coefficient of the graph obtained by

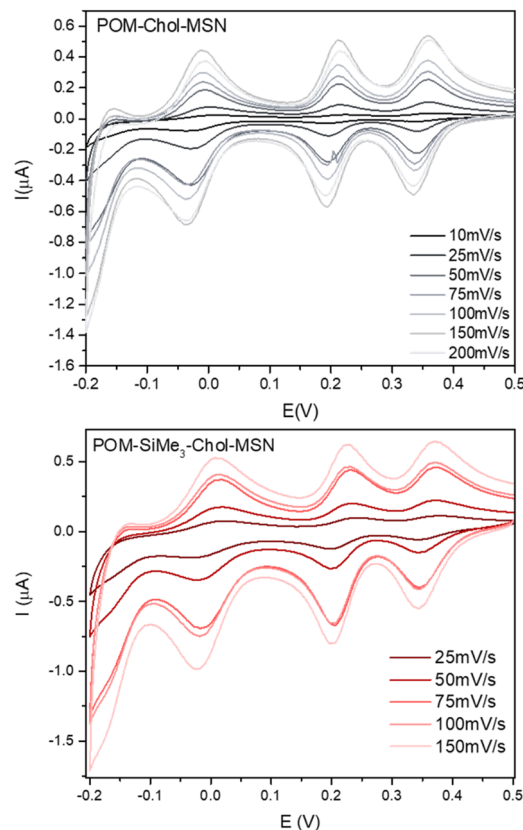


Fig. 9 Cyclic voltammograms of POM-SiMe<sub>3</sub>-Chol-MSN immobilized on a carbon-modified electrode as the working electrode in nitrogen saturated aqueous 0.5 M H<sub>2</sub>SO<sub>4</sub> *vs.* an Ag/AgCl/KCl (3 M) reference electrode and a platinum rod as the counter electrode.





plotting the current intensity of the first two peaks *versus* the scan speed ( $\nu^n$ ) improves with an  $n$  exponent lower than  $\frac{1}{2}$ . This suggests that there is no mass transport of the analyte due to the attachment of the  $[\text{PMo}_{12}\text{O}_{40}]^{3-}$  anions to the silica surface. Thus, the electron exchange rate takes place between the electrode and the anchored  $[\text{PMo}_{12}\text{O}_{40}]^{3-}$  anions. As mentioned before, the peak-to-peak separation value between  $E_{\text{cathodic}}$  and  $E_{\text{anodic}}$  increases from its theoretical value (59/2 mV) for those materials with capped silanol groups, POM-R-Chol-MSN (R = Me, Ph, SiMe<sub>3</sub>, and CH<sub>2</sub>CH<sub>2</sub>PPh<sub>2</sub>), in comparison with that of non-protected POM-Chol-MSN. It also increases with the scan speed, which suggests that the presence of silanol groups on the silica surface influences the electron transfer rate, and therefore the interaction between the heteropolyanion and the silica surface. The CV measured for H<sub>3</sub>[PMo<sub>12</sub>O<sub>40</sub>] (Fig. S11†) shows two quasi-reversible two-electron redox reactions (0.37 and 0.23 V) and a third irreversible redox process (−0.03 V), that are interpreted in terms of the hydrolysis of the reactant.<sup>31</sup>

Differential pulse voltammetry (DPV), a more sensitive technique, was used to gain insight into the changes in the reduction potential values upon immobilization (Fig. 10). In DPV experiments four cathodic peaks associated with molybdenum(vi) reduction processes were observed. DPV of POM-Chol-MSN shows a slight shift to lower potentials in the peak positions in comparison with that of free  $[\text{PMo}_{12}\text{O}_{40}]^{3-}$  (from 0.37 to 0.34 V), which means that the heteropolyanion reduces at a lower potential upon immobilization due to the increase of the electron density of the anion. The DPV of free  $[\text{PMo}_{12}\text{O}_{40}]^{3-}$  recorded in ethanol/sulfuric acid solution or sulfuric acid solution (Fig. S12†) shows important differences in the height of the peaks. For example, in the presence of ethanol the peak intensity increases gradually suggesting the

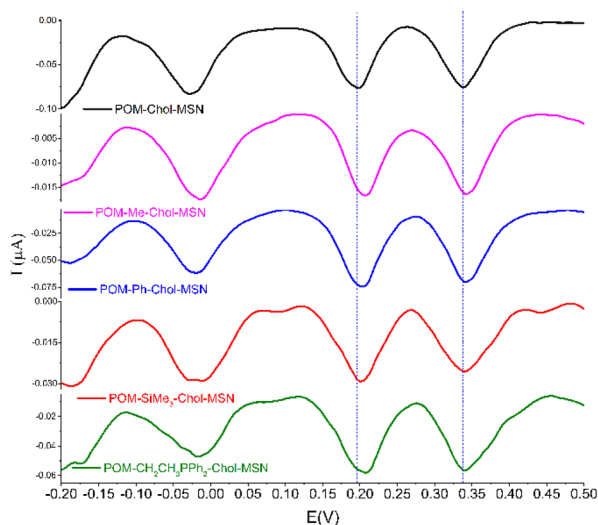


**Fig. 10** Differential pulse voltammograms of polyoxometalate-based materials using a carbon-modified electrode as the working electrode in nitrogen saturated aqueous 0.5 M H<sub>2</sub>SO<sub>4</sub> vs. an Ag/AgCl/KCl (3 M) reference electrode and a platinum rod as the counter electrode.

involvement of a higher number of electrons in the reduction processes, and hence the existence of hydrolysis. This behaviour suggests that in solution H<sub>3</sub>[PMo<sub>12</sub>O<sub>40</sub>] suffers a severe structural reorganization upon reduction, depending on the solvent. After immobilization, an electrochemical stabilization of the anion takes place. For instance, anchored  $[\text{PMo}_{12}\text{O}_{40}]^{3-}$  in POM-SiMe<sub>3</sub>-Chol-MSN has shown to be an effective electrocatalyst in the oxidation of ascorbic acid (see Fig. S13†).

**3.2.4. Evaluation of the hydrophobic/hydrophilic properties of the surface of the materials.** Impedance spectroscopy (EIS) and CV are suitable techniques for studying and monitoring the changes taking place on the silica surface as the result of the silanization reactions undertaken. EIS enables the determination of the charge transfer resistance ( $R_{\text{ct}}$ ) of the modified carbon paste electrodes, which can be interpreted as the resistance of the electrode surface towards electron transfer from  $[\text{Fe}(\text{CN})_6]^{3-/4-}$ , used as the redox probe. The EIS spectrum for the redox  $[\text{Fe}(\text{CN})_6]^{3-/4-}$  pair, obtained with the bare carbon paste electrode, is a classic example of a quasi-reversible and diffusion-controlled electron transfer process. The measurement of the charge transfer resistance,  $R_{\text{ct}}$ , is dependent on the diameter of the semicircle obtained in the Nyquist plots, the larger the diameter, the greater the charge transfer resistance. As can be seen in Fig. 11, the charge transfer resistance of the electrodes decreases when the electrodes are prepared with polyoxometalate anions anchored to the silica surface, in comparison with the bare carbon paste electrode. This can be explained in terms of the presence of POM units as electroactive species with rich redox chemistry. There are significant differences among all the materials, those functionalized with phenyl (Ph-SiO<sub>3</sub><sup>-</sup>, 7634 Ω), and (diphenylphosphine)ethyl groups (PPh<sub>2</sub>-CH<sub>2</sub>-CH<sub>2</sub>-SiO<sub>3</sub><sup>-</sup>, 7628 Ω) show the highest values of charge transfer resistance, followed by those functionalized with the trimethylsilyl groups (Me<sub>3</sub>Si-O-SiO<sub>3</sub><sup>-</sup>, 4539 Ω), and methyl groups (Me-SiO<sub>3</sub><sup>-</sup>, 4209 Ω). Finally, the unsilylated material POM-Chol-MSN (2010 Ω) shows a charge transfer value half of that of the best value obtained for

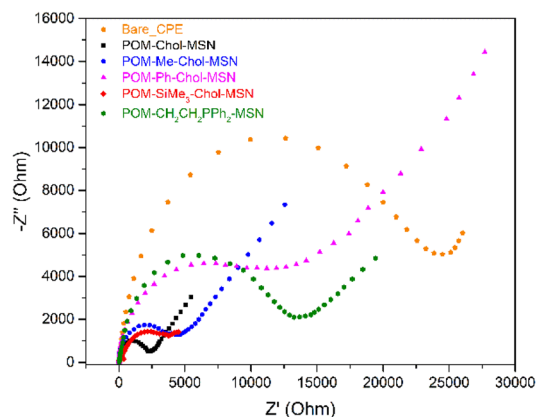


**Fig. 11** Nyquist plots showing the modification of the materials recorded in 0.5 M H<sub>2</sub>SO<sub>4</sub> containing the redox system  $[\text{Fe}(\text{CN})_6]^{3-/4-}$ .



the silylated material, and ten times less than the bare carbon paste electrode.

EIS results are in agreement with the measurements obtained for cyclic voltammetry using  $[\text{Fe}(\text{CN})_6]^{3-/4-}$  as a probe molecule (Fig. S14†). In the case of the POM-Chol-MSN, the process is highly reversible with the lowest  $\Delta E$  value and  $I_{\text{ox}}/I_{\text{red}}$  equal to one. Meanwhile, the reversibility of the redox process of the  $[\text{Fe}(\text{CN})_6]^{3-/4-}$  system decreased after surface silanization, and the  $\Delta E$  values increased by 10–30 mV, which confirms that the presence of hydrophobic groups on the silica makes the electron transfer process difficult. However, as expected, important differences are found among the materials, POM-SiMe<sub>3</sub>-Chol-MSN modified with the trimethylsilyl groups, Me<sub>3</sub>Si-O-SiO<sub>3</sub>, shows higher reversibility for the redox process, close to the non-silylated material POM-Chol-MSN.

$\zeta$  potentials of the hybrid nanoparticles were also measured from Milli-Q H<sub>2</sub>O colloidal 1 mg mL<sup>-1</sup> suspensions at pH 7. Pristine MSN are characterized by a negative  $\zeta$  potential (from -20 to -30) due to the presence of deprotonated silanol groups.<sup>32</sup> Upon functionalization with the choline hydroxide ionic liquid, the  $\zeta$  potential of choline-based silica nanoparticles increases due to the presence of a positively charged quaternary ammonium group. But it still shows negative values, which are maintained upon the immobilization of the polyoxometalate anion.  $\zeta$  potential values for the materials under study are shown in Table 1, as can be seen, the masking of silanol groups with different capping agents causes an additional decrease of  $\zeta$  potential which is an expected phenomenon for more hydrophobic particles.<sup>14,15</sup>

In addition, wettability experiments were carried out (Fig. 12). A contact angle (CA) of 59.71° was obtained when a water droplet was dropped on the surface of hybrid mesoporous silica nanoparticles, SiMe<sub>3</sub>-Chol-MSN, which indicates that the wettability of the material towards water is poor. When a water droplet was in contact with the surface of Chol-MSN a contact angle of 30.69° was observed suggesting the lower surface hydrophobicity of this catalyst. Additionally, the contact angle analysis on the surface of POM-SiMe<sub>3</sub>-Chol-MSN was also investigated. When water drops on the surface of the

catalyst, the water diffuses on the catalyst surface (Fig. 12C), showing good hydrophilicity after polyoxometalate incorporation. With a model oil as the testing droplet, the octane/DBT diffuses as well (Fig. 12D), demonstrating the amphiphilic properties of this catalyst.

### 3.3. Oxidative desulfurization of DBT: activities of the different catalysts

Desulfurization experiments with POM-based materials were carried out using 1 mol% of catalyst, 10 mL of a DBT solution (250 ppm-S) in *n*-octane, as a model oil, and with H<sub>2</sub>O<sub>2</sub> as an eco-friendly oxidant. An O/S ratio of 6 and 1 mol% of catalyst were chosen to avoid the influence of polyoxometalate dosage on the catalytical results. The oxidative desulfurization (ODS) reaction was performed without a co-solvent under mild conditions (40 °C). To corroborate that the polyoxometalate-based silicas are the active species in the catalytic process, a blank experiment was performed without the catalyst showing a conversion of DBT of 1.3% after 1 h.

Fig. 13A shows the kinetic profiles of the experiments for 1 h. The results indicate that the POM-SiMe<sub>3</sub>-Chol-MSN catalyst renders a quantitative conversion towards sulfone in 45 minutes. Table 2 presents the DBT removal efficiency of the POM-based catalysts by adsorption and catalysis processes.

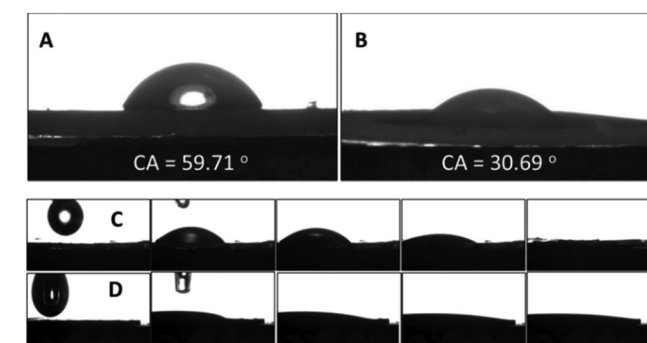
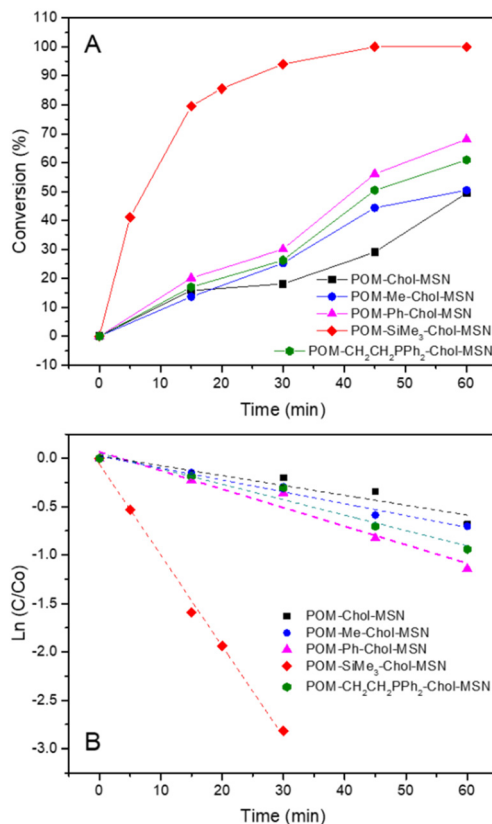


Fig. 12 The contact angle of water on the surface of (A) SiMe<sub>3</sub>-Chol-MSN (B) Chol-MSN (C) POM-SiMe<sub>3</sub>-Chol-MSN and (D) the contact angle of the model oil in POM-SiMe<sub>3</sub>-Chol-MSN.

Fig. 13 The catalytic performance of POM based materials for DBT desulfurization. (A) Kinetic profiles and (B) pseudo-first order fit for different catalysts.



**Table 2** Adsorption and conversion of DBT and constant rate values for pseudo-first order kinetics using POM-based materials

Catalyst	Adsorption <sup>a</sup> (%)	Conversion <sup>b</sup> (%)	<i>k</i> (min <sup>-1</sup> )
POM-Chol-MSN	6.5	49	-0.01023
POM-Me-Chol-MSN	1.2	50	-0.01229
POM-Ph-Chol-MSN	6.0	68	-0.01922
POM-SiMe <sub>3</sub> -Chol-MSN	81.5	100	-0.09382
POM-CH <sub>2</sub> CH <sub>2</sub> PPh <sub>2</sub> -MSN	1.0	61	-0.01597

<sup>a</sup> Experimental conditions. Adsorption experiments: 10 mL of the model oil, 1% catalyst, 1 h and 40 °C. <sup>b</sup> Catalytic test: 10 mL of the model oil, 1 mol% catalyst, 24 μL of 30% H<sub>2</sub>O<sub>2</sub> (O/S = 6). Adsorption and conversion of DBT determined by GC.

POM-Ph-Chol-MSN and POM-CH<sub>2</sub>CH<sub>2</sub>PPh<sub>2</sub>-Chol-MSN catalysts show a lower performance with 69 and 65% conversion, respectively; while POM-Me-Chol-MSN and POM-Chol-MSN show the lowest conversion values, 46 and 44%, respectively. The process takes place to render in all cases dibenzothio-phenone sulfone as the only product. Based on desulfurization efficiencies of the different materials, the reaction kinetics was studied, and the apparent rate constants associated with these catalysts were calculated using a pseudo-first order fit (Table 2 and Fig. 13B).

Previously reported studies have demonstrated that the use of ionic liquids as an extraction solvent makes possible the conciliation of liquid extraction of non-polar DBT and heterogeneous catalytic oxidation. In these materials, capping of the silanol groups on the silica surface, allows the increase of the surface hydrophobicity resulting in bimodal nanoparticles, which influences the efficiency of these materials in the ODS process. The different activity in ODS observed for POM-SiMe<sub>3</sub>-Chol-MSN reveals that trimethylsilyl groups on the silica surface improve their properties as a bimodal catalyst.

The hydrophobic nature of the POM-SiMe<sub>3</sub>-Chol-MSN material endows this material with the best properties as an adsorbent with 81.5% of adsorption, far higher than the rest of the silylated materials. The POM-Ph-Chol-MSN material, that possesses phenyl groups capable of establishing π-π stack-

ing interactions, achieves 6% adsorption.<sup>33</sup> However, the adsorption for POM-CH<sub>2</sub>CH<sub>2</sub>PPh<sub>2</sub>-Chol-MSN with available phenyl groups on the phosphine unit is essentially zero.

From the results, it can be concluded that the adsorption of DBT is a key step in the catalytic process. The POM-SiMe<sub>3</sub>-Chol-MSN catalyst, capable of adsorbing DBT and H<sub>2</sub>O<sub>2</sub> simultaneously improves considerably the oxidation and removal of DBT.

Effective catalysts based on heterogenized phosphomolybdates (Table 3) or phosphotungstates (Table S2†) are found in the literature. Comparing our results with other recently reported polyoxometalates, POM-SiMe<sub>3</sub>-Chol-MSN exhibits a complete conversion (in only 45 min) with less POM loading (7.5 wt% of theoretical H<sub>3</sub>[PMo<sub>12</sub>O<sub>40</sub>]) than the reported catalysts (20–60 wt% of theoretical H<sub>3</sub>[PMo<sub>12</sub>O<sub>40</sub>]). Zhang *et al.*<sup>34</sup> prepared the material PMA/UiO-66 with a low POM loading (10% loading), which exhibited 100% DBT conversion in 55 min but using an organic oxidant (TBHP) and at a higher temperature (80 °C). The material 10.9% HPMo/C reported by Ghubayra *et al.*<sup>35</sup> achieved a complete DBT conversion in 30 min at 60 °C. The design of hybrid mesoporous silicas with amphipathic properties has been shown to be successful in comparison with other supports used previously such as boron nitride,<sup>36</sup> organic poly(ionic liquid) hybrids,<sup>37,38</sup> hybrid magnetic mesoporous silica microspheres,<sup>39</sup> or SBA-15 prepared by our group.<sup>11</sup> The high stability offered by immobilized polyoxometalates is also significant in comparison with other molybdenum precursors.<sup>30</sup> Indeed, using POM-SiMe<sub>3</sub>-Chol-MSN the kinetic constant rose about 1.2 times higher (*k* = 0.09382 min<sup>-1</sup>) than that obtained with the reported silica@C-dots/phosphotungstate catalyst (*k* = 0.0777 min<sup>-1</sup>).<sup>40</sup> The apparent activation energy calculated from the Arrhenius equation are 33.72, 30.85 and 82.85 kJ mol<sup>-1</sup> for POM-SiMe<sub>3</sub>-Chol-MSN, POM-Chol-MSN and POM-CH<sub>2</sub>CH<sub>2</sub>PPh<sub>2</sub>-Chol-MSN, respectively, for some representative materials.

**3.3.1. Reusability of the catalyst.** To test the catalyst durability and recycling performance, repeated experiments have been conducted in the ODS of DBT for POM-SiMe<sub>3</sub>-Chol-MSN under the same conditions (1 mol% of catalyst, 250 ppm-S, O/S = 6, 40 °C, 1 h), and the results are shown in Fig. 14. After each run, the catalyst was recovered by filtration, and reused

**Table 3** Catalysts based on heterogenized phosphomolybdates for the oxidation of DBT in model diesel fuel with H<sub>2</sub>O<sub>2</sub>

Catalyst	POM <sup>a</sup> (wt%)	Model oil/ co-solvent	Catalyst dosage (g L <sup>-1</sup> )	O/S ratio	Temperature (°C)	Time (min)	Conversion (%)	Ref.
PMA/UiO-66	10	Decalin	5	3 <sup>b</sup>	80	55	100	34
10.9% HPMo/C	10.9	Heptane/H <sub>2</sub> O	7	3	60	30	100	35
HPMo/BN-IL	20	Octane	10	4	40	100	94.3	36
PDIM-PMo-W <sub>70%</sub>	60.9	Octane	4	4	50	40	100	37
PIL-Mo <sub>8</sub> O <sub>26</sub> <sup>4-</sup>	0.43 <sup>c</sup>	Dodecane	2.5	4	30	90	82.4	38
[R <sub>3</sub> NCH <sub>3</sub> ] <sub>3</sub> PMo <sub>12</sub> O <sub>40</sub> /RS-MMS	30	Dodecane	10	4	60	50	99.7	39
Mo@mSnO <sub>2</sub> (20% cat.)	20 <sup>d</sup>	Heptane/CH <sub>3</sub> CN	1.25	2.5	60	120	95	30
POM-SiMe <sub>3</sub> -Chol-SBA-15	15	Octane	5	6	40	120	93.1	11
POM-SiMe <sub>3</sub> -Chol-MSN	7.5	Octane	7.2	6	40	45	100	This work

<sup>a</sup> wt% of the theoretical POM (H<sub>3</sub>[PMo<sub>12</sub>O<sub>40</sub>]) loading. <sup>b</sup> TBHP instead of H<sub>2</sub>O<sub>2</sub>. <sup>c</sup> mmol of Mo dosage. <sup>d</sup> wt% of theoretical MoO<sub>3</sub>.



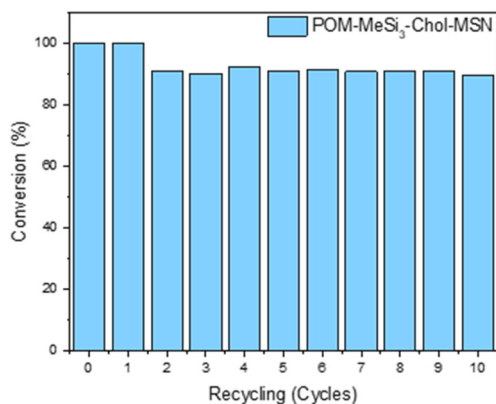


Fig. 14 The catalytic activity of POM-SiMe<sub>3</sub>-Chol-MSN in ten consecutive reaction cycles of oxidative desulfurization of DBT.

without any further treatment. The removal of sulfur for ten consecutive runs was satisfactory in terms of sulfone selectivity, exhibiting a drop in the DBT conversion value from 100 to 90% at the third run probably due to the loss of the catalyst after filtration, since from this run the DBT conversion remains constant.

### 3.4. Mechanism proposal

To gain additional insight into the catalyst's nature and stability, electrochemical studies of carbon paste electrodes modified with POM-Chol-MSN treated with H<sub>2</sub>O<sub>2</sub> and recovered after the catalysis experiment were performed (Fig. 15). Similarly, recovered POM-SiMe<sub>3</sub>-Chol-MSN was also studied. As can be seen in Fig. 15, after hydrogen peroxide treatment, the DPV recorded for POM-Chol-MSN/H<sub>2</sub>O<sub>2</sub> shows similar cathodic peaks to POM-Chol-MSN, although a slight difference in the first reduction peak is observed, it shifts from 0.34 to 0.33 V value indicating higher electron density in Mo(vi) centers due to the formation of peroxy species.

In addition, an important decrease in the peak height is observed for the third and fourth reduction steps, which suggests lower stability of the generated peroxy species. After the first catalytic run experiment, the DPV for the recovered sample shows significant differences in comparison with the fresh material. The first reduction peak potential appears now at 0.34 V, suggesting the recovery of polyoxometalate species; however, the third and fourth reduction peaks appear overlapped, that is, new Mo=O species have been generated *in situ* from supported polyoxometalate anions.

XPS of the recovered catalyst after the first run (Fig. S9†) shows that the reused catalyst contains a higher amount of the reduced molybdenum species, the Mo<sup>6+</sup>/Mo<sup>5+</sup> ratio decreases from 1.65 to 1.5, which can be attributed to the catalytic cycle due to the presence of H<sub>2</sub>O<sub>2</sub> and the substrate. DPV measured for the recovered sample after two runs confirm the nearly quantitative formation of a new Mo=O(vi) compound. As can be seen, a high current reduction peak appears at 0.11 V, alongside three consecutive reduction peaks associated with the Mo(vi) reduction in the former POM unit, probably due to

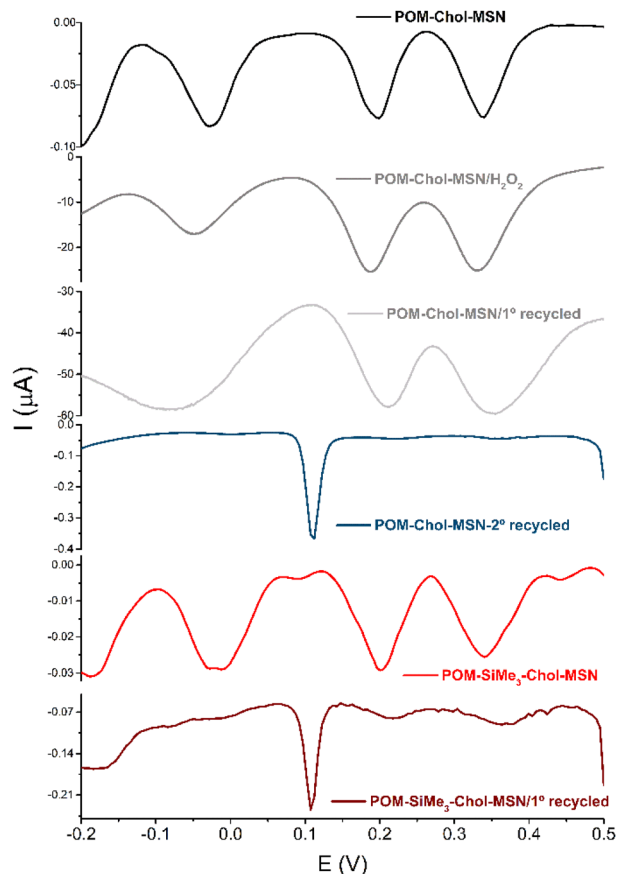


Fig. 15 DPV of POM-Chol-MSN and POM-SiMe<sub>3</sub>-Chol-MSN after two consecutive experiments immobilized on a carbon-modified electrode as the working electrode in nitrogen saturated aqueous 0.5 M H<sub>2</sub>SO<sub>4</sub> vs. an Ag/AgCl/KCl (3 M) reference electrode and a platinum rod as the counter electrode.

the presence of some untransformed POM anions (the pre-catalyst in the ODS process). The DPV conducted for POM-SiMe<sub>3</sub>-Chol-MSN recovered after two runs confirms the formation of the same catalytically active species, since the same high current peak at 0.11 V appears. FTIR of this recovered sample shows the signals attributed to the unchanged heteropolyanion and an additional signal at around 882 cm<sup>-1</sup> due to the formation of the Mo=O<sub>t</sub> (O<sub>t</sub> is terminal oxygen) species (Fig. S4†).

Finally, the CV of both recovered materials was performed and the results are summarized in Fig. 16 and Fig. S15.† The redox chemistry of the newly formed Mo=O(vi) compound is associated with an irreversible redox process with  $E_{\text{cathodic}} = 0.08$  V and  $E_{\text{anodic}} = 0.23$  V, respectively. Several proposals are found in the literature describing the reactivity of polyoxometalates with hydrogen peroxide.<sup>41</sup>

The mechanism proposed by Ishii-Venturello involves the use of heteropolyacids, H<sub>2</sub>O<sub>2</sub> as an oxidant, and a surfactant that forms a polyoxometalate/H<sub>2</sub>O<sub>2</sub> catalytic oxidation system. According to the proposed mechanism (see Fig. 17), the Keggin-POM precursor initially degrades in the presence of





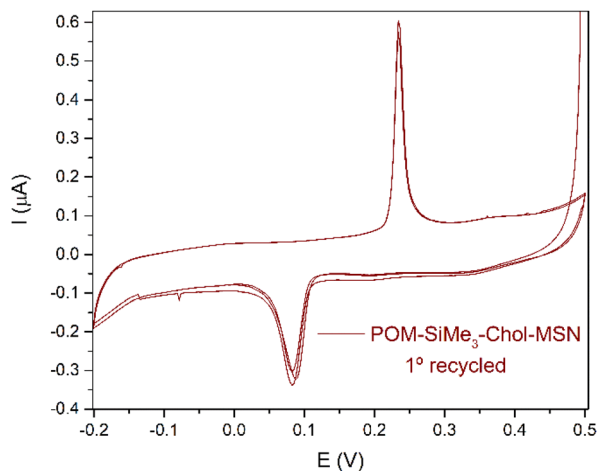


**Fig. 16** CV of POM-SiMe<sub>3</sub>-Chol-MSN recycled after two consecutive experiments, immobilized on a carbon-modified electrode as the working electrode in nitrogen saturated aqueous 0.5 M H<sub>2</sub>SO<sub>4</sub> vs. an Ag/AgCl/KCl (3 M) reference electrode and a platinum rod as the counter electrode.

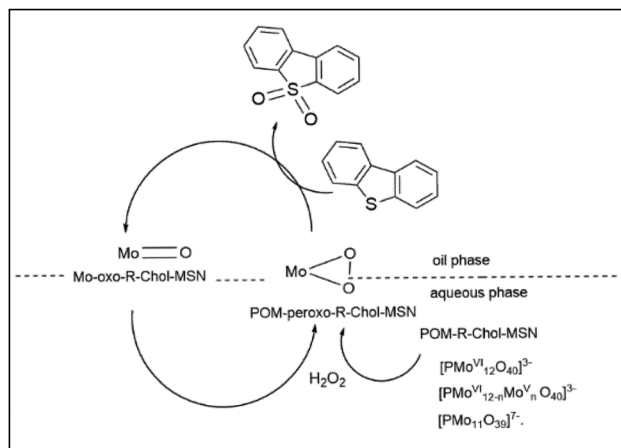


**Fig. 17** The proposed mechanism for the oxidation of DBT by H<sub>2</sub>O<sub>2</sub> catalyzed by POM-R-Chol-MSN in the model ion (two-phase) system.

H<sub>2</sub>O<sub>2</sub> to form the active peroxy species in the aqueous phase, which are highly active catalysts in the biphasic oxidation (the oxidation takes place in the organic phase). Finally, the regeneration of the active peroxy species takes place again in the aqueous phase.<sup>7,42,43</sup> According to the electrochemical measurements performed in this study, in the presence of H<sub>2</sub>O<sub>2</sub>, the immobilized and highly stabilized POM in the hybrid silica material forms an active Mo=O(vi) compound with a reduction potential of 0.11 V (measured by DPV), which becomes the active species in the catalytic process in the presence of H<sub>2</sub>O<sub>2</sub>, and that it can be regenerated up to at least ten runs without further decomposition. This transformation is nearly quantitative as shown by the low current values measured in the DPV for the peaks associated with untransformed POM. In comparison, the peak current due to the

newly formed Mo=O(vi) compound is 6.5 times higher after two runs for recovered POM-SiMe<sub>3</sub>-Chol-MSN.

## 4. Conclusions

Heterogenous catalysts with polyoxometalates immobilized on hybrid silica materials have been prepared and successfully used as ODS systems for DBT removal from oils with H<sub>2</sub>O<sub>2</sub> as a green oxidant and without co-solvent under mild conditions (1 h and 40 °C). The hybrid silicas combine hydrophilic-hydrophobic properties, which influence DBT adsorption and simultaneously allow the heterogenization of polyoxometalates as active species in the ODS process. Thus, the coverage of silica mesoporous nanoparticles with choline functionality and alkylsilyl or arylsilyl groups provides affinity to both water and water-immiscible organic phases, enabling assembly just at their interface, to drive the catalytic reaction of chemical species in both phases. Indeed, the POM-SiMe<sub>3</sub>-Chol-MSN catalyst exhibits outstanding catalytic activity (total DBT removal in only 45 min) and reusability without further treatment. <sup>31</sup>P MAS and <sup>95</sup>Mo-NMR spectroscopy and electrochemical studies concluded that the POM clusters tethered onto the mesoporous silica surface are fully accessible and interact with the unmasked surface silanol groups. Thus, the coverage of silica surface groups plays a significant role in the ODS reaction. The electronic properties of the heteropolyanion can be tuned by acting on the nature of the silica surface groups as has been demonstrated by extensive characterization of the materials.

## Conflicts of interest

There are no conflicts to declare.

## Acknowledgements

We gratefully acknowledge the financial support from the MICINN (project RTI2018-094322-B-I00).

## Notes and references

- 1 D. Julião, R. Valença, J. C. Ribeiro, B. de Castro and S. S. Balula, *Appl. Catal., A*, 2017, 537, 93–99, DOI: [10.1016/j.apcata.2017.02.021](https://doi.org/10.1016/j.apcata.2017.02.021).
- 2 H. N. Miras, J. Yan, D. Long and L. Cronin, *Chem. Soc. Rev.*, 2012, 41, 7403–7430, DOI: [10.1039/C2CS35190K](https://doi.org/10.1039/C2CS35190K).
- 3 F. M. B. Gusmão, D. Mladenović, K. Radinović, D. M. F. Santos and B. Šljukić, *Energies*, 2022, 15(23), 9021–9039, DOI: [10.3390/en15239021](https://doi.org/10.3390/en15239021).
- 4 I. Ullah, A. Munir, A. Haider, N. Ullah and I. Hussain, *Nanophotonics*, 2021, 10, 1595–1620, DOI: [10.1515/nanoph-2020-0542](https://doi.org/10.1515/nanoph-2020-0542).



- 5 H. Tao, T. Nakazato and S. Sato, *Fuel*, 2009, **88**, 1961–1969, DOI: [10.1016/j.fuel.2009.03.020](https://doi.org/10.1016/j.fuel.2009.03.020).
- 6 N. Mansir, Y. H. Taufiq-Yap, U. Rashid and I. M. Lokman, *Energy Convers. Manage.*, 2017, **141**, 171–182, DOI: [10.1016/j.enconman.2016.07.037](https://doi.org/10.1016/j.enconman.2016.07.037).
- 7 M. Craven, D. Xiao, C. Kunstmann-Olsen, E. F. Kozhevnikova, F. Blanc, A. Steiner and I. V. Kozhevnikov, *Appl. Catal., B*, 2018, **231**, 82–91, DOI: [10.1016/j.apcatb.2018.03.005](https://doi.org/10.1016/j.apcatb.2018.03.005).
- 8 W. Kaleta and K. Nowińska, *Chem. Commun.*, 2001, 535–536, DOI: [10.1039/B007111K](https://doi.org/10.1039/B007111K).
- 9 X. Li, J. Zhang, F. Zhou, Y. Wang, X. Yuan and H. Wang, *Mol. Catal.*, 2018, **452**, 93–99, DOI: [10.1016/j.mcat.2017.09.038](https://doi.org/10.1016/j.mcat.2017.09.038).
- 10 S. O. Ribeiro, B. Duarte, B. de Castro, C. M. Granadeiro and S. S. Balula, *Materials*, 2018, **11**, 1196, DOI: [10.3390/ma11071196](https://doi.org/10.3390/ma11071196).
- 11 J. Ortiz-Bustos, Y. Pérez and I. del Hierro, *Microporous Mesoporous Mater.*, 2021, **321**, 111128, DOI: [10.1016/j.micromeso.2021.111128](https://doi.org/10.1016/j.micromeso.2021.111128).
- 12 P. Cruz, Y. Pérez and I. del Hierro, *Microporous Mesoporous Mater.*, 2017, **240**, 227–235, DOI: [10.1016/j.micromeso.2016.11.028](https://doi.org/10.1016/j.micromeso.2016.11.028).
- 13 I. del Hierro, Y. Pérez and M. Fajardo, *Microporous Mesoporous Mater.*, 2018, **263**, 173–180, DOI: [10.1016/j.micromeso.2017.12.024](https://doi.org/10.1016/j.micromeso.2017.12.024).
- 14 M. Zhao, W. Lv, Y. Li, C. Dai, H. Zhou, X. Song and Y. Wu, *Materials*, 2018, **11**, 1385, DOI: [10.3390/ma11081385](https://doi.org/10.3390/ma11081385).
- 15 A. W. Carpenter, B. V. Worley, D. L. Slomberg and M. H. Schoenfish, *Biomacromolecules*, 2012, **13**, 3334–3342, DOI: [10.1021/bm301108x](https://doi.org/10.1021/bm301108x).
- 16 Y. Wei, B. Han, Z. Dong and W. Feng, *J. Mater. Sci. Technol.*, 2019, **35**, 1951–1958, DOI: [10.1016/j.jmst.2019.05.014](https://doi.org/10.1016/j.jmst.2019.05.014).
- 17 A. Duan, G. Wan, Z. Zhao, C. Xu, Y. Zheng, Y. Zhang, T. Dou, X. Bao and K. Chung, *Catal. Today*, 2007, **119**, 13–18, DOI: [10.1016/j.cattod.2006.08.049](https://doi.org/10.1016/j.cattod.2006.08.049).
- 18 J. A. F. Gamelas, A. M. V. Cavaleiro, E. de Matos Gomes, M. Belsley and E. Herdtweck, *Polyhedron*, 2002, **21**, 2537–2545, DOI: [10.1016/S0277-5387\(02\)01238-X](https://doi.org/10.1016/S0277-5387(02)01238-X).
- 19 Y. Tian, G. Wang, J. Long, J. Cui, W. Jin and D. Zeng, *Chin. J. Catal.*, 2016, **37**, 2098–2105, DOI: [10.1016/S1872-2067\(16\)62558-5](https://doi.org/10.1016/S1872-2067(16)62558-5).
- 20 X. Chang, X. Yang, Y. Qiao, S. Wang, M. Zhang, J. Xu, D. Wang and X. Bu, *Small*, 2020, **16**, 1906432, DOI: [10.1002/smll.201906432](https://doi.org/10.1002/smll.201906432).
- 21 M. Gisbert-Garzarán and M. Vallet-Regí, *Nanomaterials*, 2020, **10**(5), 916–965, DOI: [10.3390/nano10050916](https://doi.org/10.3390/nano10050916).
- 22 P. Shinde and B. L. V. Prasad, *Part. Part. Syst. Charact.*, 2021, **38**, 2100185, DOI: [10.1002/ppsc.202100185](https://doi.org/10.1002/ppsc.202100185).
- 23 J. d'Espinoza de Lacaille, F. Barberon, K. V. Romanenko, O. B. Lapina, L. L. Pollès, R. Gautier and Z. Gan, *J. Phys. Chem. B*, 2005, **109**, 14033–14042, DOI: [10.1021/jp0519621](https://doi.org/10.1021/jp0519621).
- 24 T. J. Bastow, *Solid State Nucl. Magn. Reson.*, 1998, **12**, 191–199, DOI: [10.1016/S0926-2040\(98\)00067-8](https://doi.org/10.1016/S0926-2040(98)00067-8).
- 25 J. C. Edwards, R. D. Adams and P. D. Ellis, *J. Am. Chem. Soc.*, 1990, **112**, 8349–8364, DOI: [10.1021/ja00179a020](https://doi.org/10.1021/ja00179a020).
- 26 H. Nagashima, J. Trébosc, Y. Kon, K. Sato, O. Lafon and J. Amoureux, *J. Am. Chem. Soc.*, 2020, **142**, 10659–10672, DOI: [10.1021/jacs.9b13838](https://doi.org/10.1021/jacs.9b13838).
- 27 E. Kolehmainen, in *Encyclopedia of Spectroscopy and Spectrometry*, ed. J. C. Lindon, Academic Press, Oxford, 2nd edn, 1999, pp. 834–843.
- 28 J. Cuny, S. Cordier, C. Perrin, C. J. Pickard, L. Delevoye, J. Trébosc, Z. Gan, L. L. Pollès and R. Gautier, *Inorg. Chem.*, 2013, **52**, 617–627, DOI: [10.1021/ic301648s](https://doi.org/10.1021/ic301648s).
- 29 T. Iijima, T. Yamase, M. Tansho, T. Shimizu and K. Nishimura, *Chem. Phys. Lett.*, 2010, **487**, 232–236, DOI: [10.1016/j.cplett.2010.01.040](https://doi.org/10.1016/j.cplett.2010.01.040).
- 30 A. Rajendran, H. Fan, T. Cui, J. Feng and W. Li, *J. Cleaner Prod.*, 2022, **334**, 130199, DOI: [10.1016/j.jclepro.2021.130199](https://doi.org/10.1016/j.jclepro.2021.130199).
- 31 M. Sadakane and M. Steckhan, *Chem. Rev.*, 1998, 219–238, DOI: [10.1021/cr960403a](https://doi.org/10.1021/cr960403a).
- 32 M. Sándor, C. L. Nistor, G. Szalontai, R. Stoica, C. A. Nicolae, E. Alexandrescu, J. Fazakas, F. Oancea and D. Donescu, *Materials*, 2016, **9**, 34, DOI: [10.3390/ma9010034](https://doi.org/10.3390/ma9010034).
- 33 Z. Kampouraki, D. A. Giannakoudakis, V. Nair, A. Hosseini-Bandegharai, J. C. Colmenares and E. A. Deliyanni, *Molecules*, 2019, **24**(24), 4525–4548, DOI: [10.3390/molecules24244525](https://doi.org/10.3390/molecules24244525).
- 34 X. Zhang, Z. Zhang, B. Zhang, X. Yang, X. Chang, Z. Zhou, D. Wang, M. Zhang and X. Bu, *Appl. Catal., B*, 2019, **256**, 117804, DOI: [10.1016/j.apcatb.2019.117804](https://doi.org/10.1016/j.apcatb.2019.117804).
- 35 R. Ghubayra, C. Nuttall, S. Hodgkiss, M. Craven, E. F. Kozhevnikova and I. V. Kozhevnikov, *Appl. Catal., B*, 2019, **253**, 309–316, DOI: [10.1016/j.apcatb.2019.04.063](https://doi.org/10.1016/j.apcatb.2019.04.063).
- 36 H. Ji, H. Ju, R. Lan, P. Wu, J. Sun, Y. Chao, S. Xun, W. Zhu and H. Li, *RSC Adv.*, 2017, **7**, 54266–54276, DOI: [10.1039/C7RA10697A](https://doi.org/10.1039/C7RA10697A).
- 37 S. Mao, Q. Zhou, H. Guo, M. Du, W. Zhu, H. Li, J. Pang, D. Dang and Y. Bai, *Fuel*, 2023, **333**, 126392, DOI: [10.1016/j.fuel.2022.126392](https://doi.org/10.1016/j.fuel.2022.126392).
- 38 H. Yang, B. Jiang, Y. Sun, L. Zhang, Z. Huang, Z. Sun and N. Yang, *J. Hazard. Mater.*, 2017, **333**, 63–72, DOI: [10.1016/j.jhazmat.2017.03.017](https://doi.org/10.1016/j.jhazmat.2017.03.017).
- 39 W. Jiang, H. Jia, X. Fan, L. Dong, T. Guo, L. Zhu, W. Zhu and H. Li, *Appl. Surf. Sci.*, 2019, **484**, 1027–1034, DOI: [10.1016/j.apsusc.2019.03.341](https://doi.org/10.1016/j.apsusc.2019.03.341).
- 40 Y. Zhang and R. Wang, *Appl. Catal., B*, 2018, **234**, 247–259, DOI: [10.1016/j.apcatb.2018.04.031](https://doi.org/10.1016/j.apcatb.2018.04.031).
- 41 D. Amitouche, M. Haouas, T. Mazari, S. Mouanni, R. Canioni, C. Rabia, E. Cadot and C. Marchal-Roch, *Appl. Catal., A*, 2018, **561**, 104–116, DOI: [10.1016/j.apcata.2018.05.017](https://doi.org/10.1016/j.apcata.2018.05.017).
- 42 Z. P. Pai, Y. A. Chesalov, P. V. Berdnikova, E. A. Uslamin, D. Y. Yushchenko, Y. V. Uchenova, T. B. Khlebnikova, V. P. Baltakhinov, D. I. Kochubey and V. I. Bukhtiyarov, *Appl. Catal., A*, 2020, **604**, 117786, DOI: [10.1016/j.apcata.2020.117786](https://doi.org/10.1016/j.apcata.2020.117786).
- 43 G. D. Yadav and A. A. Pujari, *Org. Process Res. Dev.*, 2000, **4**, 88–93, DOI: [10.1021/op990055p](https://doi.org/10.1021/op990055p).

